# Using the Earth's Magnetic field to constrain the Coupling Strength between Photons and Axions

David Ellis & Shane Fenn
School of Physics and Astronomy
University of Nottingham

March 5, 2019

## Abstract

Axions are a theoretical particle hypothesized as a means of solving the Charge-Parity (CP) problem of Quantum Chromodynamics (QCD) and, along with other axion-like particles (ALPs), are a strong candidate for dark matter. ALPs couple to photons with a probability of conversion proportional to the square of the magnitude and length of the perpendicular magnetic field. Current methods for detecting ALPs typically employ very large magnetic fields over short distances. In this investigation, we consider restricting our search to low mass axions to allow for photon propagation on astronomical scales while using the Earth's magnetic field to produce ALPs. We calculated the theoretical limit on the capability of constraining the coupling constant achievable using current lunar ranging technology by considering the eccentricity of the moon's orbit and found that for pseudoscalar ALPs a maximum constraint of $g_{a\gamma} < (7.2 \pm 1.9) \times 10^{-5} \text{GeV}^{-1}$ for axion masses $m_a < 10^{-7}$eV. We also consider a pair of satellites exchanging a beam of photons based on technology used in the LISA Pathfinder experiment. We demonstrate that a polar orbit would be most effective at constraining $g_{a\gamma}$ finding a maximum constraint of $g_{a\gamma} < (2.0 \pm 0.5) \times 10^{-12} \text{GeV}^{-1}$ and $g'_{a\gamma} < (4.0 \pm 1.0) \times 10^{-12} \text{GeV}^{-1}$ after a months orbit for pseudoscalar and scalar ALPs respectively for masses $m_a < 2 \times 10^{-6}$eV.

# Contents

# 1  Introduction

The axion is a hypothetical elementary particle which appears in many extensions of the standard model of particle physics. Their existence was first proposed in 1977 by Peccei and Quinn to solve the charge-parity (CP) problem of quantum chromodynamics (QCD), a problem yet to be answered within the standard model of particle physics [1]. A physical law has CP symmetry if it remains true after interchanging each particle with its antiparticle while simultaneously inverting the spatial coordinates of the system. As early as 1964, physicists have observed CP symmetry violation in electroweak interactions. However, there is no verified observation of CP violation in the strong sector. This is a type of fine-tuning problem as there is no known reason why CP symmetry should be conserved in the strong sector. The QCD Lagrangian contains a CP violating term with a coefficient proportional to

$$\bar{\theta} = \theta_{\mathrm{QCD}} + \arg \det(M_{\mathrm{quark}}), \tag{1}$$

where $\theta_{\mathrm{QCD}}$ is the $\theta$-vacuum and $M_{\mathrm{quark}}$ is the quark mass matrix [2]. A non-zero value for $\bar{\theta}$ would result in the neutrino having an electric dipole moment. However, the absence of such a dipole moment has been confirmed to a precision of $d_{\mathrm{n}} < 3.0 \times 10^{-23}\ e$ cm [3]. The theory developed by Peccei and Quinn, known as PQ theory, proposes altering the QCD Lagrangian by considering $\bar{\theta}$ as a dynamic field

$$\bar{\theta} = \frac{a(\mathbf{x})}{f_a}, \tag{2}$$

where $a(\mathbf{x})$ is the axion field and $f_a$ is the axion decay constant. This dynamic field is a pseudo-Goldstone boson field which arises from the breaking of a global U(1) symmetry caused by the vacuum expectation values of a scalar field.

Low mass axions $m_a < 0.1\mathrm{eV}/c^2$, as well as many other very weakly interacting slim particles (WISPs) may have been produced non-thermally in the early universe via a mechanism called vacuum-misalignment [4]. Vacuum misalignment is an effect hypothesised in PQ theory which occurs when a particles field has an initial value which is not located near a potential minimum. This produces an oscillation in the particles field around the nearest minima, radiating energy via decay processes until the minimum is reached. This causes the CP-violating coefficient to tend towards a near-zero value, therefore explaining the lack of observed CP-violation. Due to their long lifetimes and weak couplings to particles of the standard model, these particles are prominent dark matter candidates [5].

Although the axion was first hypothesised in 1977, there has been a recent resurgence of interest due to lack of evidence of Weakly Interacting Massive Particles (WIMPs) from both particle collider experiments and direct detection experiments [6][7]. The axion hypothesized by Peccei and Quinn is a pseudo-scalar Goldstone Boson. However, many other axion-like particles (ALPs) have also been predicted by Type IIB string theory including both scalar and pseudoscalar variants [8] [9].

The effective Lagrangian density of photons and axions is given by

$$\mathcal{L} = -\frac{1}{4}F_{\mu\nu}F^{\mu\nu} - \frac{1}{2}(\partial_\mu a \partial^\mu a - m_a^2 a^2) - \frac{1}{4}g_{a\gamma}a F_{\mu\nu}\tilde{F}^{\mu\nu}, \tag{3}$$

where $a$ is the axion field, $m_a$ is the axion mass, $g_{a\gamma}$ is the coupling constant, $F_{\mu\nu} = \partial_\mu A_\nu - \partial_\nu A_\mu$ is the electromagnetic field tensor and $\tilde{F}^{\mu\nu} = \frac{1}{2}\epsilon_{\mu\nu\rho\sigma}F^{\rho\sigma}$ is the dual of the electromagnetic field tensor where $\epsilon_{\mu\nu\rho\sigma}$ is defined as

$$\epsilon_{\mu\nu\rho\sigma} = \begin{cases} +1 & \text{if } (\mu,\nu,\rho,\sigma) \text{ is an even permutation of (1,2,3,4)} \\ -1 & \text{if } (\mu,\nu,\rho,\sigma) \text{ is an odd permutation of (1,2,3,4)} \\ 0 & \text{otherwise} \end{cases} . \tag{4}$$

The final term in (3) indicates that we expect a three vertex interaction involving a single axion and two photons. With the strength of this particle coupling being given by $g_{a\gamma}$. Due to this coupling, it is possible for an axion to convert into a photon via the Primakoff production method in stars [10] or alternatively and more relevant to our investigation, an axion may be converted to a photon and vice-versa in the presence of an inhomogeneous magnetic field. The magnetic field acts as an electromagnetic background which supplies the additional virtual photon required for the conversion. The field must be inhomogeneous as to provide the three-momentum necessary to change a spin-1 photon into a spin-0 axion [11]. For pseudoscalar axions and ALPs, the probability of this conversion is found to be

$$P_{a\leftrightarrow\gamma} = \left( \frac{g_{a\gamma} B \sin(\theta)}{q} \sin\left( \frac{qL}{2} \right) \right)^2 , \tag{5}$$

where $B$ is the magnetic field strength, $\theta$ is the angle between the field and the direction of the photon beam, $L$ is the distance of magnetic field that the photon propagates through and $q$ is the axion-photon momentum transfer in a vacuum [12]. In a vacuum, the momentum transfer is given by

$$q = \frac{m_{\mathrm{a}}^2}{2\omega}, \tag{6}$$

where $\omega$ is the photon frequency [13]. For scalar ALPs, equation (5) is modified by replacing $g_{a\gamma}\sin(\theta)$ with $g'_{a\gamma}\cos(\theta)$, in which $g'_{a\gamma}$ is the coupling between the photon and scalar ALPs. Equation (5) is simplified the limit $qL/2 \ll 1$ for $\theta = \pi/2$ as this allows us to remove the $\sin(\theta)$ and $\sin\left( \frac{qL}{2} \right)$ terms. The equation then becomes

$$P_{a\leftrightarrow\gamma} = \left( \frac{g_{a\gamma} BL}{2} \right)^2 . \tag{7}$$

Equation (7) shows that, in the limit of small axion masses, the conversion probability is equally dependent on the square of both the magnetic field strength and the length of the magnetic field through which the photon propagates. These two factors are central to the majority of modern axion searching experiments.

## 2    Current Research

Due to the predicted low mass of axions, it is not possible to detect them directly as is currently being performed in an attempt to detect WIMPs [14]. Instead, experiments focus on detecting them indirectly through their coupling with photons.

### 2.1    Haloscopes

If axions form at least a substantial component of our galaxies dark matter halo, it is expected that there will be a large flux of axions passing through the Earth at all times. Therefore, if we present these axions with an inhomogeneous magnetic field then we should

expect to observe some of them convert into photons [11] through the coupling given by equation (5).

Currently, the leading haloscope experiment is the Axion Dark Matter eXperiment (ADMX). In this experiment, a superconducting solenoid is used to generate a 7.6T magnetic field. A resonant microwave cavity is then used to detect photons converted from axions found in our galaxy's dark matter halo [15]. Based on assumptions regarding the density and distribution of dark matter within our galaxy, the excluded region of axion parameter space, shown in figure 1, is produced.

As can be seen from figure 1, this type of experiment is limited in the range of axion masses it can constrain. Furthermore, if axions do not make up any fraction of the dark matter at all, the haloscope method becomes completely redundant.

## 2.2   Helioscopes

As discussed, axions should be produced in the sun through processes such as the Primakoff effect. Helioscope experiments aim to detect these axions by aiming a dipole magnet towards the Sun to collect axions produced through solar emission. The magnetic field then provides the virtual photons required for the coupling. The photons produced following the conversion process are then detected.

To date, the most sensitive helioscope is the CERN Axion Space Telescope (CAST) collaboration [16]. This experiment uses a 9T refurbished test magnet from the Large Hadron Collider [13]. The experiment is only able to maintain coherence in the limit $qL/2 \ll 1$. Therefore, to be able to constrain the coupling constant for axion masses up to $m_a \approx 10^{-2}$eV, the field length, $L$, must be small. This limits the probability of conversion that is obtainable. The area of the coupling-mass parameter space excluded by CAST is shown in figure 1. CAST currently produces the best constraints on the coupling constant between photons and pseudoscalar ALPs of any experiment, constraining the coupling to within $g_{a\gamma} < 0.66 \times 10^{10}$GeV$^{-1}$. As such, this value will be used as a benchmark for our own results.

The International AXion Observatory (IAXO) is proposed to be the successor to CAST. Its purpose-built dipole magnet will utilise an axion-sensitive area around 1500 times larger than that used by CAST. Additionally, IAXO will be able to track the sun across the sky for around 12 hours a day, four times longer than that of its predecessor. These combined features allow IAXO to achieve sensitivities four to five times greater than CAST, relating to more than an order of magnitude improvement in the constraints on the coupling constant, constraining it to within $g_{a\gamma} \lesssim 3 \times 10^{-12}$ GeV$^{-1}$ [17]. The predicted exclusion of the coupling-mass parameter space is compared to the current limits imposed by CAST in figure 1.

The key drawback of helioscope experiments is that they rely on the Primakoff process occurring in the sun and the resulting axions or ALPs being emitted towards the detector. This introduces an element of uncertainty to the experiment that cannot be easily controlled. Additionally, due to the direction of the magnetic field used by both CAST and IAXO, these experiments are unable to constrain the coupling strength between photons and scalar ALPs.

## 2.3   Light Shining through a Wall

Both the haloscope and helioscope method exhibit similar problems; their ability to infer the presence of axions is dependent on either dark matter being composed of axions or axions being produced in the sun. The strength of 'Light Shining through a Wall' (LSW) experiments

is that their ability to infer the presence of ALPs is dependent only on the existence of the particle and their coupling to photons.

In these experiments, a laser beam is directed at a classically opaque wall in the presence of a strong magnetic field. There is then a small probability that some of these photons will be converted into axions and pass through the wall due to their weak coupling to matter of the standard model. Once they have passed through the wall, it is possible for these axions to revert back into photons which can then be detected.

Currently, the best limits produced by a LSW experiment are set by the Any Light Particle Search (ALPS) experiment, constraining the coupling strength to within $g_{a\gamma} \lesssim 7 \times 10^{-8} \text{GeV}^{-1}$ ($m_a \lesssim 10^{-3}$eV) for both scalar and pseudoscalar ALPs [12]. This sensitivity is around three orders of magnitude worse than the constraints imposed by CAST. This sensitivity will, however, be greatly improved upon by its successor ALPS-II, which is predicted to achieve sensitivity down to $g_{a\gamma} \lesssim 2 \times 10^{-11} \text{GeV}^{-1}$ ($m_a \lesssim 10^{-3}$eV) which surpasses the limits imposed by CAST [18]. These experiments provide the best constraints on the photons coupling to scalar axion-like particles and therefore will be used as our benchmark for this type of constraint.

Axions and ALPs are not the only theoretical particles that can be inferred this way. As such, LSW experiments also provide constraints on the existence of hidden photons and minicharged particles. The primary drawback of this type of experiment, however, is the requirement that the axion-photon conversion must take place twice for the event to be detectable. This makes detecting the event much less likely.

## 3 Astronomical Constraints

### 3.1 Stellar Evolution

There are a number of mechanisms through which axions could be produced within stars. One such process is the Primakoff effect

$$\gamma + Ze \to Ze + a. \tag{8}$$

Axions produced this way would carry energy away from the star similarly to thermal neutrinos. The lifetime of stars can, therefore, provide an indication of the efficiency of these process and therefore the axion mass. From this we can infer the limit $m_a \lesssim 0.4$eV as shown in figure 1 [19].

### 3.2 Supernova Core Collapse

Neutrinos take a very long time to escape the supernova core after collapse due to the extreme pressures and temperatures. However, as with their emission from stars, axions would carry energy away from the inner core. This energy loss would impart an observable effect on the emitted neutrinos. The duration of the neutrino signal from a supernova, therefore, provides a limit on the coupling between axions and nucleons [19]. This argument is invalidated however if the coupling between axions and nucleons is strong enough to prevent many axions from escaping.
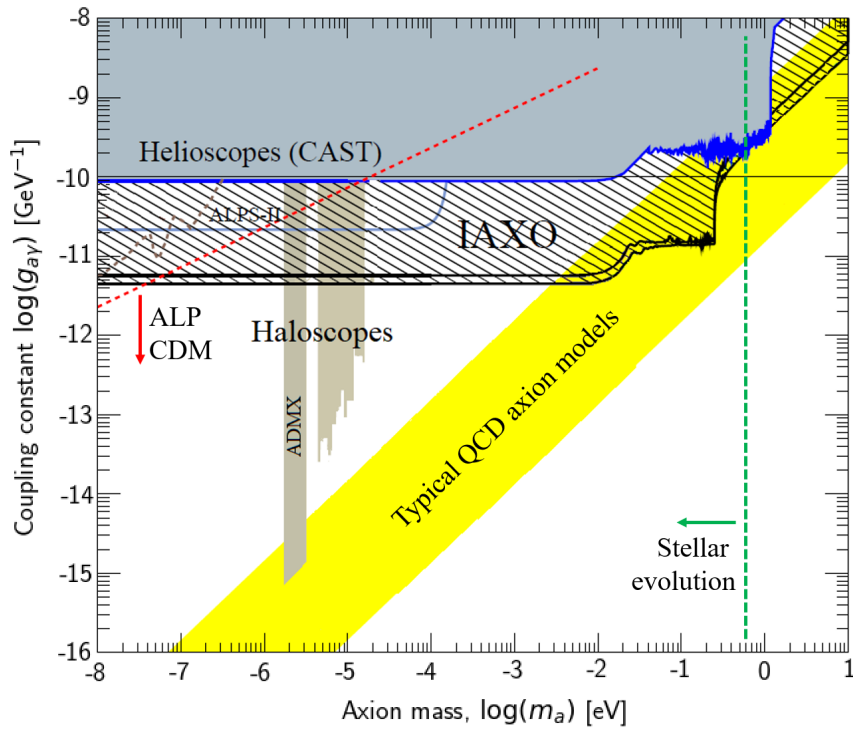
Figure 1: $g_{a\gamma}$-$m_a$ parameter space including region excluded by CAST and area expected to be excluded by IAXO. Diagonal yellow band: Typical QCD axion models defined roughly for $m_a f_a \approx m_\pi f_\pi$. The area below the red dashed line is viable ALP dark matter parameter space. The area to the right of the green dashed line is excluded by stellar evolution considerations. Figure modified from [16].

# 4   Our Concept

The current axion searching methods primarily rely on increasing the axion production probability by employing a very strong magnetic field over relatively short distances. The limitation of many of these experiments arises from the technical challenge of producing magnets powerful enough to generate the required fields. Equation (7) shows us that in the low mass regime we may be able to use a weaker magnetic field over a larger distance to produce probabilities and therefore constraints that may surpass those from other experiments. The advantage of this approach is that instead of generating a magnetic field ourselves, we can make use of the geomagnetic field produced in the Earths core. Although the strength of this field is only on order of tens of microtesla, the scale of the field allows us to transmit photon beams over much greater distances through the weaker magnetic field. This opens possibilities for new methods of indirect axion detection.

Unfortunately, due to the inhomogeneous nature of the geomagnetic field at large scales, it is not possible to use equation (7) to accurately calculate the axion conversion probability over these large distances. Instead, we will have to develop a method that addresses the inhomogeneity of the magnetic field as well as considering the two-way nature of the conversion process, as some axions may convert back into photons after their initial conversion. The logical starting place is the Lagrangian density of axions and photons given by equation (3).

## 4.1   Theory

If we apply the Euler-Lagrange equations to (3) then we recover the Klein-Gordon equation

$$(\partial_\mu^2 - m_a^2)a = \frac{1}{4}g_{a\gamma\gamma}F_{\mu\nu}\tilde{F}^{\mu\nu}. \tag{9}$$

For our system, consisting of a photon beam propagating through a magnetic field, the electromagnetic field $A$ has two components, a background magnetic field and a perturbation to this field caused by the photon propagation. This allows us to write $A$ as a sum of these two components, $A_\mu = A_{\mu B} + A_{\mu\gamma}$ where $A_{\mu B}$ and $A_{\mu\gamma}$ are the background magnetic field and photon propagation components of $A_\mu$ respectively. When we expand $F_{\mu\nu}\tilde{F}^{\mu\nu}$ we may use the fact that the effect of the photon perturbation on the field will be small allowing us to neglect $A_\gamma$ terms higher than first order. We also make the gauge choice that $A_0 = 0$ to obtain

$$\begin{aligned}
F_{\mu\nu}\tilde{F}^{\mu\nu} = 4[&\partial_0 A_{1B}(\partial_2 A_{3B} - \partial_3 A_{2B} + \partial_2 A_{3\gamma} - \partial_3 A_{2\gamma}) + \partial_0 A_{1\gamma}(\partial_2 A_{3B} - \partial_3 A_{2B}) \\
&+\partial_0 A_{2B}(\partial_3 A_{1B} - \partial_1 A_{3B} + \partial_3 A_{1\gamma} - \partial_1 A_{3\gamma}) + \partial_0 A_{2\gamma}(\partial_3 A_{1B} - \partial_1 A_{3B}) \\
&+\partial_0 A_{3B}(\partial_1 A_{2B} - \partial_2 A_{1B} + \partial_1 A_{2\gamma} - \partial_2 A_{1\gamma}) + \partial_0 A_{3\gamma}(\partial_1 A_{2B} - \partial_2 A_{1B})],
\end{aligned} \tag{10}$$

which, if we consider a constant magnetic field and therefore set $\partial_0 A_{\mu B} = 0$, can be simplified to

$$\begin{aligned}
F_{\mu\nu}\tilde{F}^{\mu\nu} = 4[&\partial_0 A_{1\gamma}(\partial_2 A_{3B} - \partial_3 A_{2B}) \\
&+\partial_0 A_{2\gamma}(\partial_3 A_{1B} - \partial_1 A_{3B}) \\
&+\partial_0 A_{3\gamma}(\partial_1 A_{2B} - \partial_2 A_{1B})].
\end{aligned} \tag{11}$$

This can be further simplified by recognising that $B_i$ is given by the curl of $A$ through the equation $(\nabla \times \underline{A})_i = \epsilon_{ijkl}\partial_j A_k$ and writing the background magnetic field terms $A_{\mu B}$ in terms of the magnetic field $B$ to find

$$F_{\mu\nu}\tilde{F}^{\mu\nu} = 4[(\partial_0 A_{1\gamma} + \partial_0 A_{2\gamma} + \partial_0 A_{3\gamma})B_0]. \tag{12}$$

Since the photon-axion interaction only occurs in the presence of a perpendicular magnetic field it is convenient to write the field $A$ as a plane wave in terms of the field components that are either perpendicular or parallel to the magnetic field such that for the case of a photon propagating in the $z$ direction

$$\underline{A}(z,t) = i \begin{bmatrix} A_x(z) \\ A_y(z) \\ A_z(z) \end{bmatrix} e^{-i\omega t} = i \begin{bmatrix} A_\parallel(z) \\ A_\perp(z) \\ 0 \end{bmatrix} e^{-i\omega t}, \tag{13}$$

where $A_\parallel$ and $A_\perp$ are the parallel and perpendicular components of $A$ respectively. We may also write the axion field as a plane wave $a(z,t) = a(z)e^{-i\omega t}$. Next, to find the equations of motion for this system we use the wave equation in which we have set $a(z) = e^{ikz}$, $a(t) = e^{i\omega t}$ to obtain

$$\frac{\partial^2 a(t)}{\partial t^2} - \frac{\partial^2 a(z)}{\partial x_i^2} = 2\omega(\omega - i\partial_z)a(z,t), \tag{14}$$

where we have used $\omega^2 + \partial_z^2 = (\omega + i\partial_z)(\omega - i\partial_z)$ and the dispersion relation $\omega \approx k$. Substituting equation (14) into the Klein-Gordon equation produces the first equation of motion

$$\left[(\omega - i\partial_z) - \frac{m_a^2}{2\omega}\right]a = -\frac{1}{2}g_{a\gamma}BA_\parallel. \tag{15}$$

The remaining equations of motion are calculated in a similar way and with the introduction of the term $\underline{\Psi}$ where

$$\underline{\Psi} = \begin{bmatrix} A_\perp(z) \\ A_\parallel(z) \\ a(z) \end{bmatrix}, \tag{16}$$

we may write the equations of motion in matrix form as

$$i\frac{\mathrm{d}\underline{\Psi}}{\mathrm{d}z} = \left[\omega - i\partial_z + \underline{M}\right] \begin{bmatrix} A_\perp(z) \\ A_\parallel(z) \\ a(z) \end{bmatrix}, \tag{17}$$

where

$$\underline{M} = \begin{bmatrix} 0 & 0 & 0 \\ 0 & 0 & \frac{1}{2}g_{a\gamma}B \\ 0 & \frac{1}{2}g_{a\gamma}B & -\frac{m_a^2}{2\omega} \end{bmatrix}. \tag{18}$$

However, we must now take into account the effect of the Euler-Heisenberg Lagrangian

$$\frac{\alpha^2}{90m_e^4}\left[(F_{\mu\nu}F^{\mu\nu})^2 + \frac{7}{4}(F_{\mu\nu}\tilde{F}^{\mu\nu})^2\right], \tag{19}$$

which is added to the earlier Lagrangian (3) as an extra term where $\alpha = e^2/4\pi$ and $m_e$ is the electron mass. The addition of this term changes the matrix $\underline{M}$ to

$$\underline{M} = \begin{bmatrix} \nabla_\perp & 0 & 0 \\ 0 & \nabla_\parallel & \nabla_m \\ 0 & \nabla_m & \nabla_a \end{bmatrix}, \tag{20}$$

where $\nabla_\perp = 2\omega\xi\sin^2(\Theta)$, $\nabla_\parallel = \frac{7}{2}\omega\xi\sin^2(\Theta)$ and $\nabla_a = -\frac{m_a^2}{2\omega}$ are the momentum differences between the respective modes and that of a photon of the same energy in a vacuum and $\nabla_m = \frac{B}{2}{}_{a\gamma}\sin(\Theta)$ is the off-diagonal component. These momentum differences are dependant on $\xi = \alpha\frac{1}{45\pi}\frac{B}{B_{\text{crit}}}^2$ which is related to the refractive indices of polarisation [20], the critical magnetic field strength $B_{\text{crit}} = \frac{m_e^2}{e}$ and $\Theta$, the angle between the external field direction and the photon momentum. It is worth noting here, that for the case of a scalar in place of a pseudoscalar axion $\underline{M}$ is analogous upon the exchange of the $\nabla_\parallel$ and $\nabla_\perp$ terms. However, for this calculation we shall consider only the pseudoscalar axion. Since we are working in the simple single domain model only the parallel component of the field $A_\parallel$ mixes with the axion. Therefore, we may ignore the perpendicular field term $A_\perp$ in $\underline{M}$ and reduce (4.1) to the 2 x 2 matrix

$$\underline{M} = \begin{bmatrix} \nabla_\parallel & \nabla_m \\ \nabla_m & \nabla_a \end{bmatrix}, \tag{21}$$

which may be diagonalised by a rotation matrix to give the resulting field strengths

$$\begin{bmatrix} A'_\parallel \\ a' \end{bmatrix} = \begin{bmatrix} \cos(\theta) & \sin(\theta) \\ -\sin(\theta) & \cos(\theta) \end{bmatrix} \begin{bmatrix} A_\parallel \\ a \end{bmatrix}. \tag{22}$$

The strength of the mixing is given by the ratio of the off-diagonal terms of $\underline{M}$ to the difference of the diagonal terms, $\theta = \frac{\nabla_m}{\nabla_\parallel - \nabla_a}$ or for the weak mixing case where $\theta \ll 1$

$$\frac{\tan(2\theta)}{2} = \frac{\nabla_m}{\nabla_\parallel - \nabla_a}. \tag{23}$$

This can be simplified if we measure the phases of all modes relative to the unmixed parallel component $A_\parallel$. Therefore, if we define the terms

$$\nabla'_\parallel = \frac{\nabla_\parallel + \nabla_a}{2} + \frac{\nabla_\parallel - \nabla_a}{2\cos(2\theta)}, \tag{24}$$

$$\nabla'_a = \frac{\nabla_\parallel + \nabla_a}{2} - \frac{\nabla_\parallel - \nabla_a}{2\cos(2\theta)}, \tag{25}$$

and neglect the common phase $e^{i(wt-wz-\nabla_\parallel z)}$ we find the following result

$$\begin{bmatrix} A_\parallel(z) \\ a(z) \end{bmatrix} = \underline{\mathcal{M}}(z) \begin{bmatrix} A_\parallel(0) \\ a(0) \end{bmatrix}, \tag{26}$$

where

$$\underline{\mathcal{M}} = \begin{bmatrix} \cos(\theta) & -\sin(\theta) \\ \sin(\theta) & \cos(\theta) \end{bmatrix} \begin{bmatrix} e^{-i(\nabla'_\parallel - \nabla_\parallel)z} & 0 \\ 0 & e^{-i(\nabla'_a - \nabla_\parallel)z} \end{bmatrix} \begin{bmatrix} \cos(\theta) & \sin(\theta) \\ -\sin(\theta) & \cos(\theta) \end{bmatrix}. \tag{27}$$

We have modelled our system in such a way that the magnetic field is uniform across the photon propagation length. This, however, this is not the case for the systems that we shall be investigating. This problem is resolved by splitting the whole field length $z$ into many smaller segments of length $dz$ over which the field is assumed to be constant. The magnitude of the perpendicular component of the magnetic field across each segment is calculated and from this, the amplitude of $A_\parallel(z)$ and $a(z)$ can be found after the distance $dz$. This is then repeated across the desired length, using the amplitude from the end of the prior segment as the initial amplitude for the next using equation (27). There are two distinct methods that we have chosen to investigate, with the aim being to study how viable they are for improving the constraints on the coupling constant $g_{a\gamma}$.

## 4.2   Lunar Laser

The first method we consider is the emission of a beam of photons from the Earth to the moon. The beam is then reflected and returned to Earth by the reflectors on the lunar surface which form part of the lunar laser ranging experiments [21]. There are a total of five reflectors on the lunar surface placed by American astronauts and Soviet rovers. These are used to calculate the Earth-Moon distance to high precision. The primary purpose of these experiments is to test Einstein's theory of general relativity. However, since the laser beams propagate through the Earth's magnetic field, some photons may be lost due to the productions of axions or ALPs. Once the photons are collected on their return to Earth, if there is a significant reduction in the number of photons detected this may indicate that axion or ALP production has occurred. The main challenge with this method is that photon loss cannot be attributed purely to axion conversion, atmospheric interference and beam divergence will also contribute to a reduction in photon count. In order to make this a more viable method, we use the fact that the radius of the lunar orbit changes over the course of a month due to its eccentricity. This periodic modulation in the distance of photon propagation will change the conversion probability and therefore should produce a detectable pattern in the photon count that is independent of the other sources of photon loss.

## 4.3   Satellite-Satellite laser

For the second method, we consider a pair of satellites with a fixed distance of separation, orbiting the Earth, with one emitting photons that are detected by the other. Again, due to the geomagnetic field, the photons may convert into axions resulting in fewer photons being detected than is expected. However, similar to the lunar laser experiment we are unable to isolate the source of photon loss as being purely down to axion production, although we will have more control over certain variables.

We consider two distinct orbits; a polar orbit, in which the satellites pass over both Earth's magnetic poles and an equatorial orbit, in which the satellites orbit the Earth around the equator. For the polar orbit, there will be a large modulation in the component of the geomagnetic field that is perpendicular and parallel to the photon beam. The perpendicular field component is greatest at the poles and falls to near zero at the equator. The opposite is true for the parallel field component. If axions are being produced then this should provide a periodic change in the detected photon count over the course of a complete orbit. This would be a clear 'smoking gun' for the presence of a coupling between photons and axion. Additionally, since the photon beam also experiences a modulated parallel magnetic field this method can also be used to constrain the photon coupling to scalar ALPs.

For an equatorial orbit, the effect of solar wind causes a difference in the geomagnetic field strength between the side of the Earth facing the sun and the side which is facing away. Again, this difference in field strength should produce an observable signal in the photon count as the satellite orbits between the two sides of Earth.

## 5  Modelling Photon Loss

Since both methods considered involve measuring the change in the number of photons it is important to maximise the number of photons that are expected in the absence of the photons coupling to axions. To do this we require a firm understanding of how many photons will be lost through non-conversion processes. The two main sources of photon loss will be due to atmospheric interference and beam divergence. The beam divergence can be characterised by the radius of the beam after travelling a certain distance. The radius $\phi$ of a Gaussian beam after propagating a distance $L$ through a vacuum is given by

$$\phi = \frac{2L\lambda}{\pi D}, \tag{28}$$

where $\lambda$ is the wavelength of light being considered and $D$ is the diameter of the primary mirror used for emission [22]. However, if we consider a beam travelling through the atmosphere the limit of diffraction is most affected by the Fried parameter $r_0$ which depends on the local atmospheric conditions and is a function of wavelength proportional to $\lambda^{\frac{6}{5}}$. This changes the beam radius such that $\phi_{2\lambda} = 2\phi_\lambda/2^{\frac{6}{5}}$. For the case where the beam is perpendicular to the Earth's surface the Fried parameter is given by

$$r_0 = \left[0.423k^2 \int_{\text{path}} C_n^2(z)dz\right]^{-\frac{3}{5}}, \tag{29}$$

where $k = 2\pi/\lambda$ is the wavenumber and $C_n^2$ is the atmospheric turbulence strength along the path of the beam, $z$. When the beam is at a zenith angle $\zeta$ the Fried parameter is $r_0 = (\cos\zeta)^{\frac{3}{5}} r_0(\zeta = 0)$. The atmospheric turbulence strength can only be found accurately through experimental data as it depends on the local conditions that are subject to change. However, relatively crude estimates suitable for this initial investigation can be found by using the mathematical Hufnagel-Valley model

$$C_n^2(h) = 5.94 \times 10^{-53} \frac{v^2}{27} h^{10} e^{(-h/1000)} + 2.7 \times 10^{-16} e^{(-h/1500)} + A e^{(-h/100)}, \tag{30}$$

where $h$ is the height at which $C_n^2$ is to be calculated for, $A$ is the relative strength of the turbulence at ground level and $v$ represents the wind speed at higher altitudes [23]. For general purposes these variables are typically given values of $A = 1.7 \times 10^{-14} \text{m}^{-2/3}$ and $v = 21 \text{m.s}^{-1}$ [24].

The moon follows an elliptical orbit around the Earth with a semi-major axis $a = 384.40 \times 10^3$km and an eccentricity $e = 0.054900$ [25]. The time-averaged distance between the centres of the Earth and Moon is 385km but due to the elliptical nature of the orbit, this distance varies between $356.5 \times 10^3$km and $406.7 \times 10^3$km every 27.5 day period. There are smaller oscillations of 3700km and 2955km to the lunar orbit every 31.8 days and 14.76 days respectively. However, for the purpose of this investigation shall only include only the larger monthly oscillation. To

ensure that our findings from the analysis of these experimental methods are based on currently achievable technology and not unfeasible performance parameters we have, where appropriate, chosen to model our parameters on existing experiments.

For the lunar laser investigation, the performance capabilities of the Apache Point Observatory Lunar Laser-ranging Operation (APOLLO) was used as a reference. APOLLO uses a 2.3W laser to generate light of wavelength 532nm in 100ps pulses with a 20Hz repetition rate. The APOLLO telescope has an aperture of 3.5m and is situated in New Mexico at an altitude of 2.8km [26]. For our investigation, we simplify the system by assuming that the telescope is based at the Earth's equator at sea level and the lunar reflector is based at the Moon's equator, which is modelled as being directly above the telescope. This allows us to use equation (5) without needing to consider with angular effects on divergence.

Assuming standard atmospheric turbulence, APOLLO produces a beam divergence on the scale of a few arcseconds. This results in a beam diameter of 1.9km at the lunar surface with the photon distribution across this area close to Gaussian in profile. This means that only around one in every $25 \times 10^6$ photons that are initially launched reach the small reflector on the lunar surface. There are numerous reflectors of various sizes and efficiency's on the surface so for our investigation we have used the performance parameters of the APOLLO 11 reflector since this is the reflector that results in the largest number of photons being returned. APOLLO 11 consists of 100 silica corner cube reflectors, each with diameter 3.8cm. The corner cubes of this reflector return the photons with a divergence of 7.5 arcseconds, resulting in a beam diameter of 15km once the beam returns to Earth. From this, an aperture of 1m will collect, on average, 1 in $2 \times 10^8$ returning photons. Together, this results in only around 1 in every $10^{16}$ emitted photons being detected after the journey. For APOLLO, only around 3775 photons are recorded every minute [21]. Assuming a night of measurements lasts 5 hours, a total of $11.3 \times 10^5$ photons will be measured during this period.

We must also establish how many photons will be lost to non-conversion processes and can be detected for the case of a laser emitted and detected by a pair of satellites. In order to ground our experiment in reality we chose to use the performance parameters of the Laser Interferometer Space Antenna (LISA) Pathfinder experiment. LISA is an interferometer designed to be capable of searching for gravitational waves. Planned for launch in 2034, LISA consists of three spacecraft arranged in an equilateral triangle of sides $2.5 \times 10^6$km. LISA Pathfinder was a proof-of-concept mission launched in 2015 to test the technologies needed for LISA. The minimum altitude of the Pathfinder spacecraft at any time is 500km [27]. The laser used by LISA has a power of 20 mW and produces light of wavelength 1064nm, which is detected by a 40cm diameter telescope [28]. The advantage of the satellite experiment is that we have greater control over some of the parameters such as altitude and the distance that the laser travels. Equation (7) shows us that for the greatest probabilities of axion production we want to maximise both the length and the magnetic field strength. This results in a need to compromise between increasing the length of the system and passing the beam as close to the Earth as possible without the losing photons to the atmosphere. It is important to avoid the beam propagating through the atmosphere as this will increase the level of beam divergence and photon absorption thus reducing the number of photons we are able to detect. Although the magnetic field will be significantly weaker, we have chosen to match the lowest altitude of LISA of $500$ km as this enables us to safely ignore the effects of atmospheric turbulence. The outgoing beam of LISA has a half cone divergence of 1.6 μrad. This means that we may separate the satellites by a maximum distance of 125km before having to consider the loss of photons due to beam divergence. This allows us to increase the number of photons detected

while also simplifying the calculations.

For the satellite experiment, we want to observe a modulation in the number of photons being detected as the satellites orbit the Earth. To make this difference as large as possible, we have chosen to only collect data from the satellites at the points of maximum and minimum strength of the relevant magnetic field component. We simplify our model by neglecting the tilt of the Earth's axis relative to its heliocentric orbital radius. For the polar case, the maximum field strength will be found above either of the poles and the minimum field strength will be above the equator. These correspond to an angles of $\theta = \pm \pi/2$ radians from the equator for the maximum points and angles of $\theta = 0, \pi$ radians for the minimum points. The parallel field maxima and minima are offset by $pi/2$ radians to those of the perpendicular field. For the equatorial orbit, the points of maximum and minimum magnetic field strength will depend largely on the angle we choose for the solar wind to approach the Earth. Again, a compromise must be made between increasing the time spent gathering photons, and therefore a greater number and having the largest difference between the conversion probabilities. We have chosen to only consider photon collection when the satellite pair is within 1% of the maximum and minimum conversion probability. To determine the size of this region a model for the magnetic field surrounding the Earth must first be developed.

# 6    Modelling the Geomagnetic Field

To estimate the constraining capability of experiments using the Earth's magnetic field, a simple model of the magnetic field surrounding the Earth was developed. This model is calculated by summing the contributions of the geomagnetic dipole field $\boldsymbol{B}_{\mathrm{Dipole}}$ with the field generated by the solar wind interacting with the Earth's magnetosphere $\boldsymbol{B}_{\mathrm{SW}}$. The total field is then given by

$$\boldsymbol{B} = \boldsymbol{B}_{\mathrm{Dipole}} + \boldsymbol{B}_{\mathrm{SW}}. \tag{31}$$

## 6.1    Dipole Field

Due to it's electrically conducting fluid core, the Earth produces a magnetic field very similar to that of a simple dipole magnet [29]. The contribution of this field dominates the total field at the low altitudes considered within this investigation. The dipole magnetic field can be approximated as the sum of radial and angular components $B_r$ and $B_\theta$ respectively where

$$B_r = -2B_0 \left( \frac{R_E}{r} \right)^3 \cos \theta, \tag{32}$$

and

$$B_\theta = -B_0 \left( \frac{R_E}{r} \right)^3 \sin \theta, \tag{33}$$

in which $B_0$ is the magnitude of the magnetic field at the equator, $r$ is the distance from the centre of the Earth, $\theta$ is the angle from the magnetic North pole and $R_E$ is the radius of the Earth [30].

To determine the value for $B_0$ the World Magnetic Model (WMM) was used. This is an empirical model of the Earth's magnetic field developed by the National Geophysical Data

Center and the British Geological Survey. This model was used through a single-point web calculator provided by the group to calculate the Northern component of the Earth's magnetic field $B_N$ as a function of the longitude as shown in figure 2 [31]. The uncertainty in the WMM field is 138nT and was therefore not plotted due to its negligible size.
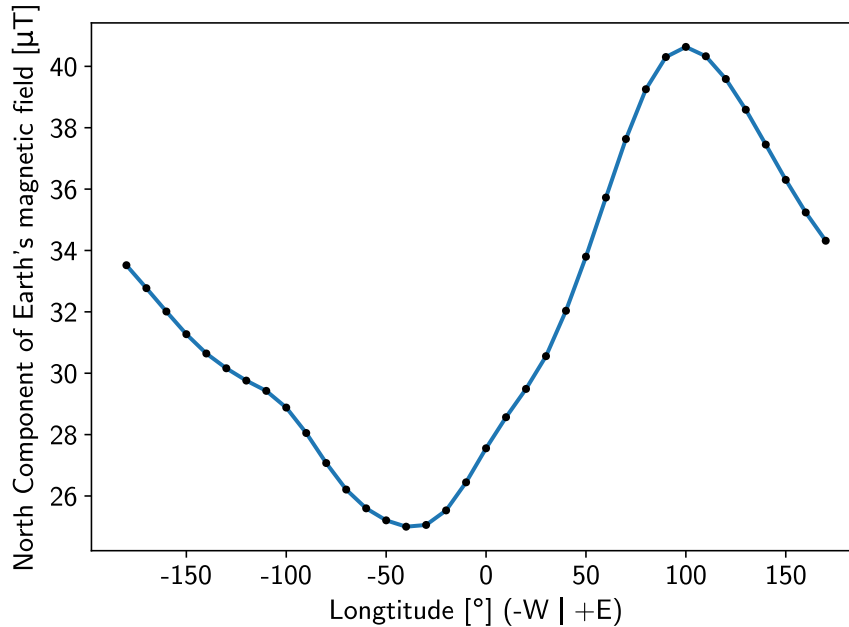


Figure 2: Northern component of the magnetic field as a function of the longitude calculated using the World Magnetic Model

The dipole equatorial field $B_0$ was found by calculating the mean of the Northern field component shown in figure 2 with variation in this field being used to quantify the error. A value of $B_0 = 31.9^{+8.7}_{-6.9}\mu$T was determined. The magnetic field due to the dipole approximation of equations (32) and (33) is compared to that of the WMM in figure 3. The WMM points are calculated above the equator at a longitude of 40° east since the Northern field component at this point is very close to the mean.

## 6.2 Solar Wind

The solar wind is composed of charged particles, the net motion of which also generates a magnetic field. Although the magnitude of the magnetic field produced by the solar wind at the altitudes we consider is much less than that of the geomagnetic field, including its effects enables us to consider the satellite equatorial orbit and adds a level of detail to the model. The flow of charged particles is largely restricted to outside of the magnetopause. The magnetopause is the boundary between the magnetosphere and the plasma emitted from the Sun. The size of the magnetopause is characterised by the Chapman-Ferarro distance. This is the distance from the Earth along the heliocentric radius at which the magnetic pressure of the geomagnetic field balances the solar wind pressure and is given by

$$R_{\mathrm{CF}} = R_{\mathrm{P}} \left( \frac{B^2_{\mathrm{surf}}}{\mu_0 \rho V^2_{\mathrm{SW}}} \right)^{1/6}, \tag{34}$$
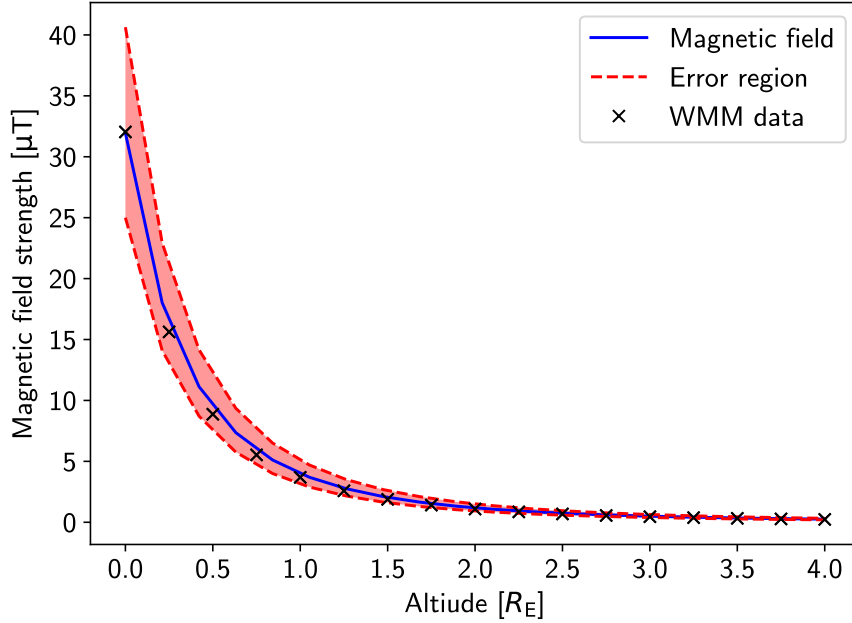
Figure 3: Comparison of the northern component of the magnetic field as calculated using the dipole approximation of and as calculated using the WMM data as a function of altitude.

where $R_{\mathrm{P}}$ is the planetary radius, $B_{\mathrm{surf}}$ is the field strength at the equator, $\rho$ is the solar wind density, $\mu_0$ is the magnetic constant and $V_{\mathrm{SW}}$ is the velocity of the solar wind [32]. At one astronomical unit from the sun, the solar wind has a velocity of $V_{\mathrm{SW}} = 468^{+242}_{-148}$ km s$^{-1}$ with a proton number density $n_{\mathrm{p}} = 8.7^{+11.3}_{-5.3}$ cm$^{-3}$ [33]. For the Earth, the Chapman-Ferarro distance is measured to be around $10.4 R_E$.

Since we are neglecting the tilt of the Earth's axis, we define x, y and z as Cartesian coordinates in which z is in the direction from the Sun to the Earth, y is along the Earth's axis and x is in the direction perpendicular to y and z.

The solar wind can be modelled as an incompressible fluid flowing over a Rankine half body. This is a fluid flow solution composed of the superposition of the solutions for the linear flow of a stream $\phi_{\mathrm{stream}}$ and the spherical flow from a source $\phi_{\mathrm{source}}$ such that

$$\phi = \phi_{\mathrm{stream}} + \phi_{\mathrm{source}}. \tag{35}$$

The stream source has a velocity potential of

$$\phi_{\mathrm{stream}} = V_{\mathrm{SW}} z \tag{36}$$

and the spherical flow from a source has a velocity potential of

$$\phi_{\mathrm{source}} = \frac{m}{2\pi} \ln\sqrt{x^2 + y^2 + z^2}, \tag{37}$$

where $m$ is the strength of the source flow. This produces a total velocity potential of

$$\phi = V_{\mathrm{SW}} z + \frac{m}{2\pi} \ln\sqrt{x^2 + y^2 + z^2}. \tag{38}$$
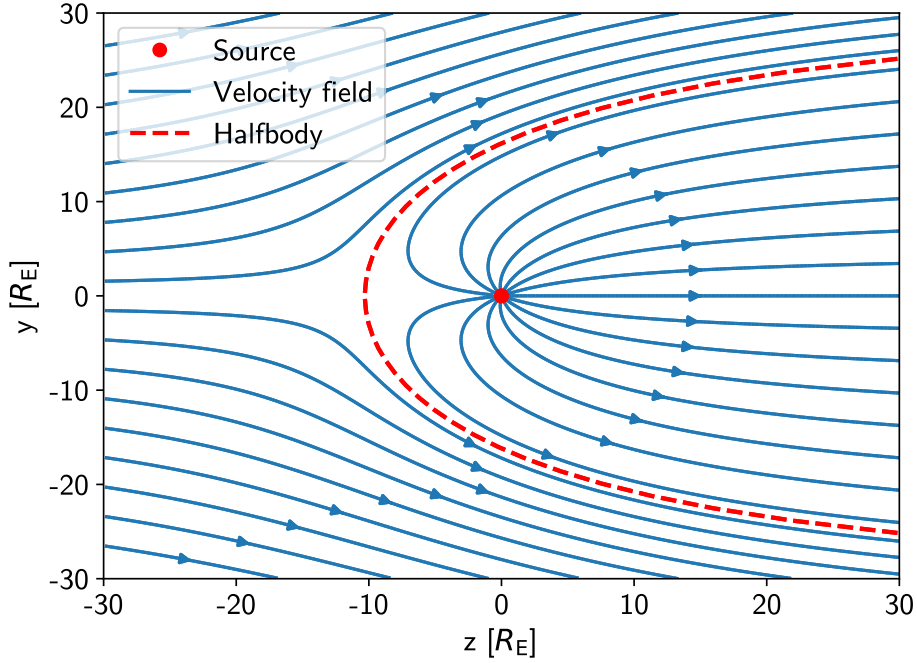
16

Figure 4: Velocity field solution for magnetopause modelled as a Rankine halfbody. The velocity field within the halfbody, shown as a red dashed line, is set to zero.

The velocity is then calculated by differentiating the velocity potential

$$v_{x_i} = \frac{\partial \phi}{\partial x_i}. \tag{39}$$

To model the magnetosphere we require that the velocity is zero at $(0, 0, -R_{\mathrm{CF}})$. This allows us to define the strength of the source $m$ to be

$$m = 2\pi V_{\mathrm{SW}} R_{\mathrm{CF}}. \tag{40}$$

A cross-section of the total flow solution for a Rankine halfbody is presented in figure 4. The absence of charged particles within the magnetopause is then imposed by requiring that within the half body the velocity is zero.

The magnetic field generated by the solar wind is then calculated. This is done by separating the considered space into $N$ segments in each direction, giving a total of $N^3$ segments each of volume $V$, where segment $i$ has a mean particle flow velocity $\vec{v}_i$. The magnetic field produced by segment $i$ at a point $P$ separated by vector $\vec{R}_{i,P}$ is then given by the Biot-Savart Law

$$\vec{B}_{i,P} = \frac{\mu_0 e n_{\mathrm{p}} V}{4\pi \mid \vec{R}_{i,P} \mid^3} \vec{v}_i \times \vec{R}_{i,P}, \tag{41}$$

where $e$ is the electron charge. The total magnetic field produced by the solar wind is then given by the sum of the contributions of each segment

$$\boldsymbol{B}_{SW} = \sum_{i=1}^{N^3} \vec{B}_{i,P} = \frac{\mu_0 e n_{\mathrm{p}} V}{4\pi} \sum_{i=1}^{N^3} \frac{\vec{v}_i \times \vec{R}_{i,P}}{\mid \vec{R}_{i,P} \mid^3}. \tag{42}$$

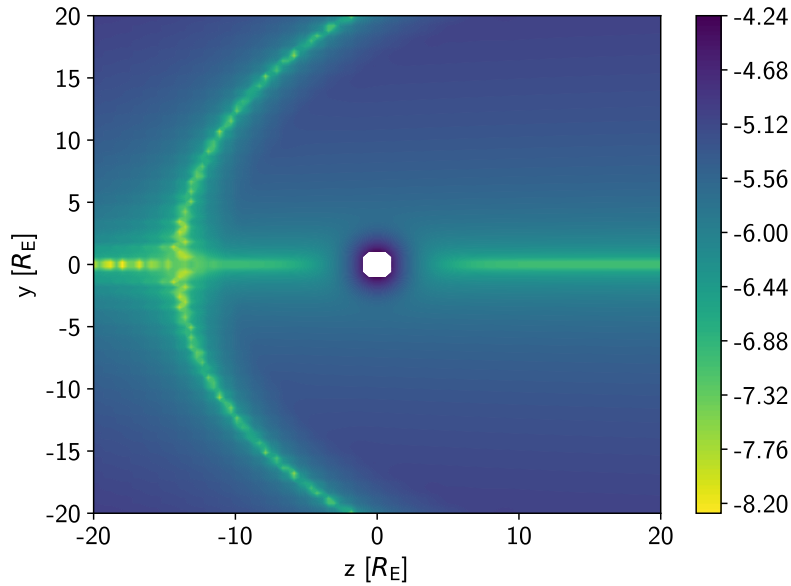Figure 5: Colour map of the magnitude of the magnetic field $\log|\mathbf{B}|$ in the y-z plane calculated by combining the dipole field generated in the Earth's core with the field produced by the flow of the solar wind over the magnetopause.

Combining the field contribution from the solar wind calculated using equation (42) with the dipole equation given by equations (32) and (33) we are able to calculate an approximate magnetic field around the Earth as shown in figure 5. The complete process for calculating the total magnetic field is outlined in the flow diagram in figure 6.

Using this method we are able to calculate the magnetic field incident on our photon beams. Due to the shape of the Earth's dipole field, a beam exchanged between a pair of satellites in a polar orbit experiences a significant magnetic field both parallel and perpendicular to it. Therefore, constraints can be generated for both scalar and pseudoscalar ALPs from a polar orbit. The average absolute value for the magnetic field perpendicular and parallel to the photon beam for a satellite pair with an altitude of 500km and a 125km separation in a polar orbit is shown in figure 7. We see that the perpendicular field varies by around $50\mu$T and around $25\mu$T for the parallel field. An experiment of this type is, therefore, better at constraining pseudoscalar ALPs than scalar ones. The primary source of error is the error in the value for the dipole equatorial field $B_0$.

An identical pair of satellites in an orbit over the Earth's equator, however, experiences a negligible parallel field and can therefore only provide constraints on pseudoscalar ALPs. The average field strength perpendicular to the beam is shown in figure 8. For this orbit, we see that the perpendicular field varies by around $2.4\mu$T. Here, the primary error is a combination of the errors on $B_0$, the proton density $n_p$ and the solar wind velocity $V_{SW}$. The size of this error is more a result of the variability of the solar weather rather than uncertainty in the calculation. It can be seen that a polar orbit should produce more significant results than an equatorial orbit due to the larger variation in both parallel and perpendicular magnetic fields and would also be more reliable since there is less uncertainty in the generation of this field.

Referring back to section 5 we may now calculate how many photons the satellite exper-

iments will be able to detect. At an altitude of 500km, the satellites will have a velocity of 7.6km s$^{-1}$. We find that this results in the satellites being within 1% of the maximum or minimum conversion probabilities for a total of 567 seconds each orbit. During this time period, a 20mW laser emits $6.07 \times 10^{19}$ photons.
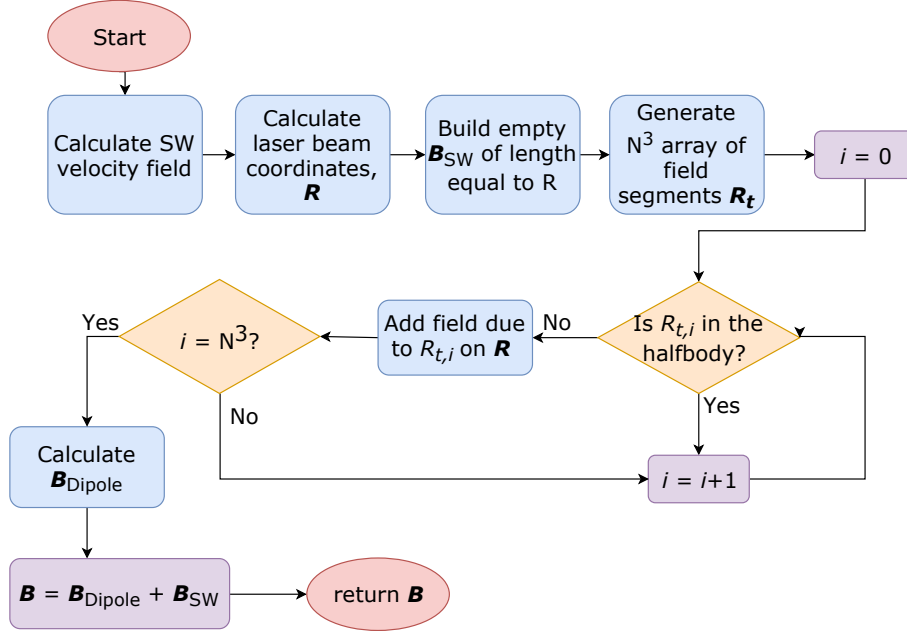


Figure 6: Flow diagram for computer code that calculates the magnetic field due to the solar wind and the Earth's dipole field.

# 7   Generating constraints

We have modelled two different systems in which the photons emitted from a laser have a chance of converting into axions or ALPs. For the lunar laser experiment, this probability varies due to the length of the beam changing. In the satellite experiment, it is the modulation of the magnetic field strength that causes the probability to change, while the beam length remains fixed. The variation in the conversion probability results in different numbers of photons being detected. To quantify the potential constraining capability of these methods we need to be able to relate the change in the number of photons detected to the axion-photon coupling constant $g_{a\gamma}$.

If we expect $N_{\mathrm{exp}}$ photons to be detected in the absence of a photon-axion coupling, with a counting error of $\sigma$ then to be able to detect a difference in the number of photons that are detected we require that

$$\Delta P N_{\mathrm{exp}} > \sigma, \tag{43}$$

where $\Delta P$ is the difference between the maximum and minimum production probability

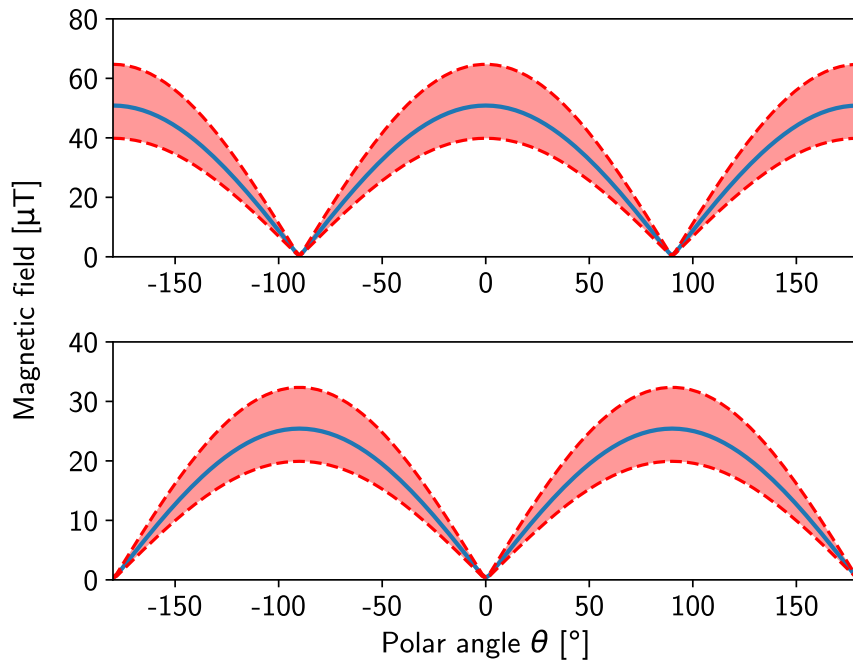$$\Delta P = P_{\mathrm{max}} - P_{\mathrm{min}}, \tag{44}$$

Figure 7: Mean absolute value for the magnetic field perpendicular (top) and parallel (bottom) to the photon beam exchanged between two satellites at an altitude of 500km, separated by 125km orbiting the Earth in a polar orbit.
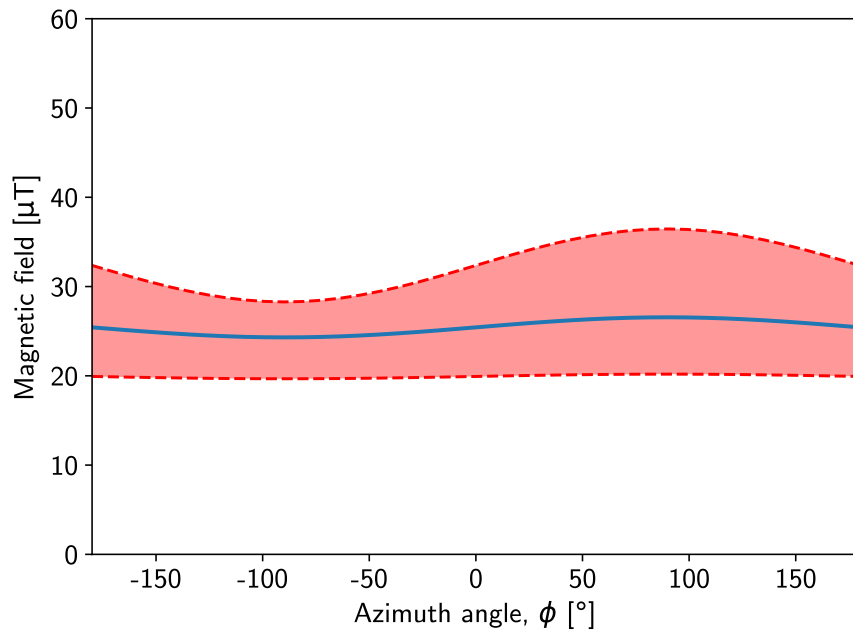


Figure 8: Mean absolute value for the magnetic field perpendicular to the photon beam exchanged between two satellites at an altitude of 500km, separated by 125km orbiting the Earth in an equatorial orbit.
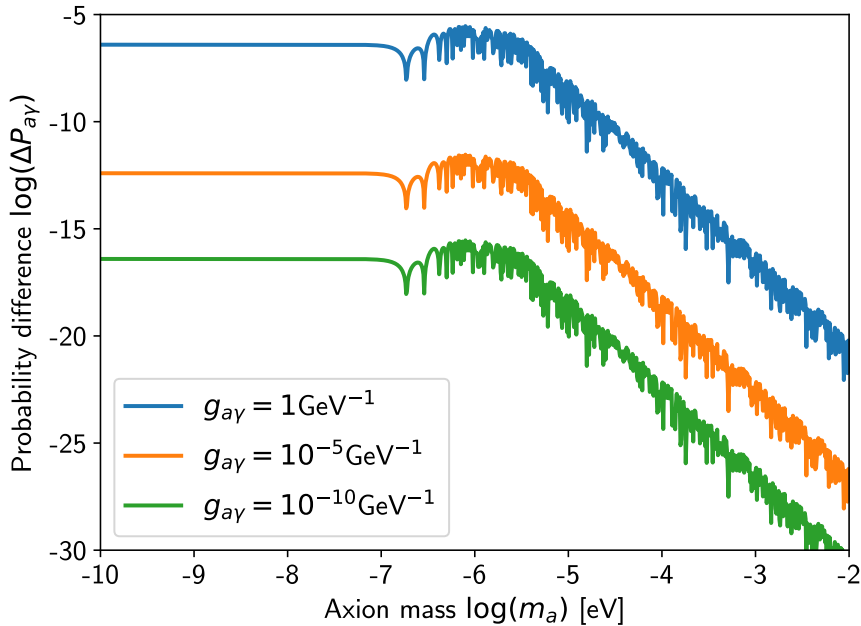
Figure 9: Difference in probability of axion production between photon beams reflected off the moon at its highest and lowest orbital radius as a function of axion mass $m_a$ for three different coupling constant $g_{a\gamma}$ values.

Since we are looking for the best constraint that is theoretically possible we make the assumption that the detectors are sensitive enough to notice the difference of a single photon. Equation (43) therefore becomes

$$\Delta P N_{\text{exp}} > 1. \tag{45}$$

Figure 9 demonstrates, for the case of the lunar laser, how the difference in axion production probability $\Delta P$ changes with the coupling constant. The sharp drops and steady decline in probability are due to the angular terms present in equation 27. Therefore, by using a bisector searching algorithm it is possible to find the smallest coupling constant that fulfils the requirement for detection defined by equation (45).

First, the magnetic field is calculated along the paths that provide the largest and smallest probabilities for photon conversion, $B_{\text{max}}$ and $B_{\text{min}}$ respectively.

Initially the lower limit for the search $g_{\text{down}}$ is set to zero and the upper limit $g_{\text{up}}$ is set to $10^{-12}$. Test values for the coupling constant are given by the mean of the upper and lower limits

$$g_{a\gamma} = \frac{1}{2}(g_{\text{up}} + g_{\text{down}}) \tag{46}$$

This value is then used to calculate the conversion probability along the paths of highest and lowest magnetic field strength, $P(B_{\text{max}})$ and $P(B_{\text{min}})$ respectively by using the conversion matrix. We then check if this fulfils the requirement for detection defined by equation (45). If not then we increase the value of $g_{\text{up}}$. This is repeated until the requirement is fulfilled to ensure that the 'true' value lies within the lower and upper bounds.

Next, we want to ensure that this value is as close to the true value of $g_{a\gamma}$ as possible. This is done by systematically moving $g_{\text{up}}$ and $g_{\text{down}}$ until the difference between $\Delta P N$ and the error $\sigma$ is less than 1% of the error value. Once this condition is met then we have found

the value for the coupling constant to within the desired precision. The full process is also outlined in the flow diagram of figure 10.
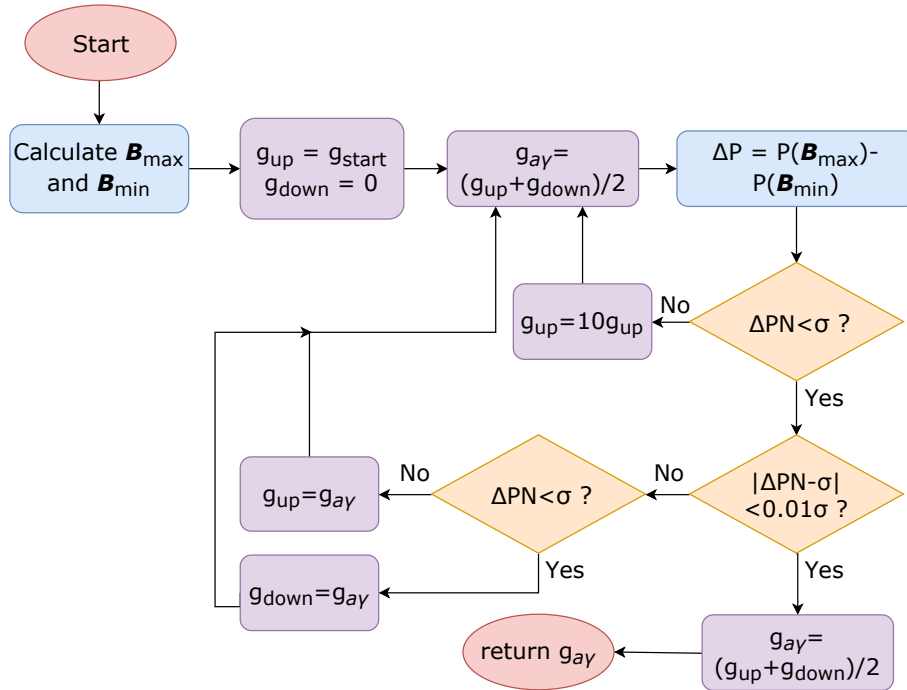


Figure 10: Flow diagram outlining the process used to calculate the smallest coupling constant required to generate a detectable difference in photons.
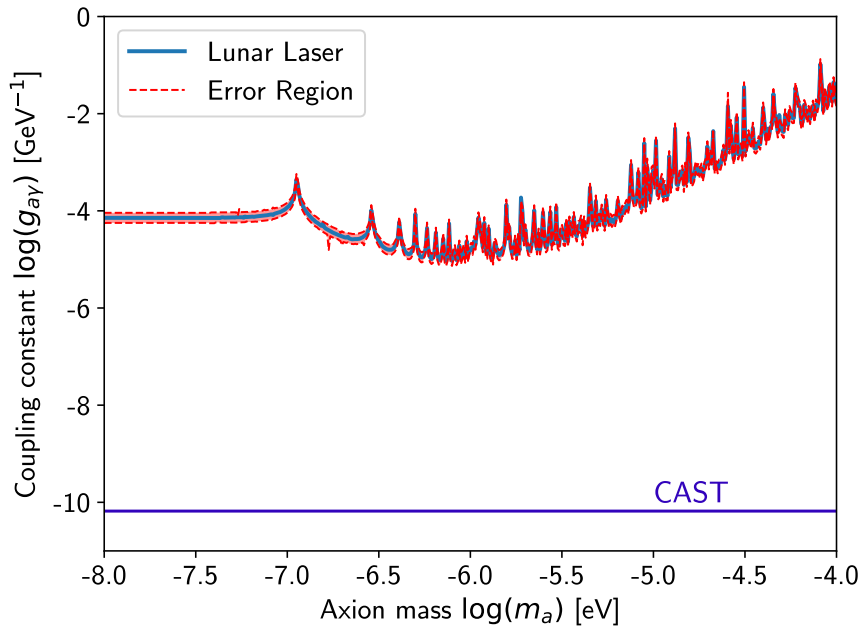
Figure 11: Minimum coupling strength $g_{a\gamma}$ able to produce a single photon difference in photon detection between the maximum and minimum lunar orbital radius for approximately five hours of detection in each configuration as a function of axion mass $m_a$

# 8    Results

## 8.1    Lunar Laser

Using the experimental parameters of APOLLO lunar ranging experiment, the bisector searching algorithm described was used to determine the best theoretical constraints that could be imposed on the axion-photon coupling constant. This limit is calculated as a function of axion mass as shown in figure 11.

From figure 11 we see that the theoretical best limit for current lunar laser technology is $g_{a\gamma} < (7.2 \pm 1.9) \times 10^{-5} \text{GeV}^{-1}$ in the low mass regime. The peaks seen starting at $m_a \approx 10^{-7}$eV are due to the angular terms in equation 27 as discussed for figure 9. Since the coherence of the longer path length is lost at a smaller axion mass than the other, there is a small dip in the constraint.

Since APOLLO measures around 1 photon for every $10^{16}$ sent, it can be estimated that they would have to use a $2 \times 10^{11}$ W laser to generate constraints equal to that of CAST.

## 8.2    Satellite-Satellite Laser

Again, by finding the coupling constant that fulfils the $N\Delta P > 1$ requirement, it is possible to estimate the maximum constraint possible using the satellite method for both a polar and an equatorial orbit. This was done for both a single orbit and a month of orbit. For the polar satellite case the theoretical best limit based on the technology used by the LISA Pathfinder experiment for scalar ALPs is $g'_{a\gamma} < (4.0 \pm 1.0 \times 10^{-12\prime})$ after a month of orbit, as shown in 12. The maximum constraint on pseudoscalar ALPs after a month of orbit for the polar case is shown in figure 13 to be $g_{a\gamma} < (2.0 \pm 0.5 \times 10^{-12})$.
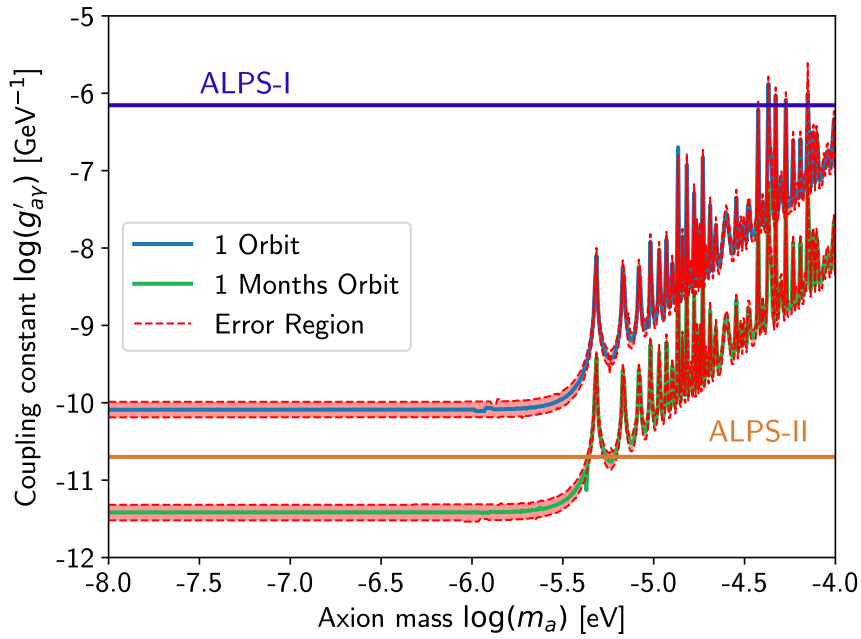
Figure 12: Minimum coupling strength $g_{a\gamma}$ able to produce a single photon difference in photon detection for scalar ALPs after a single orbit and a month of polar orbit as a function of axion mass $m_a$.



Figure 13: Minimum coupling strength $g_{a\gamma}$ able to produce a single photon difference in photon detection for pseudoscalar ALPs after a single orbit and a month of polar orbit as a function of axion mass $m_a$.
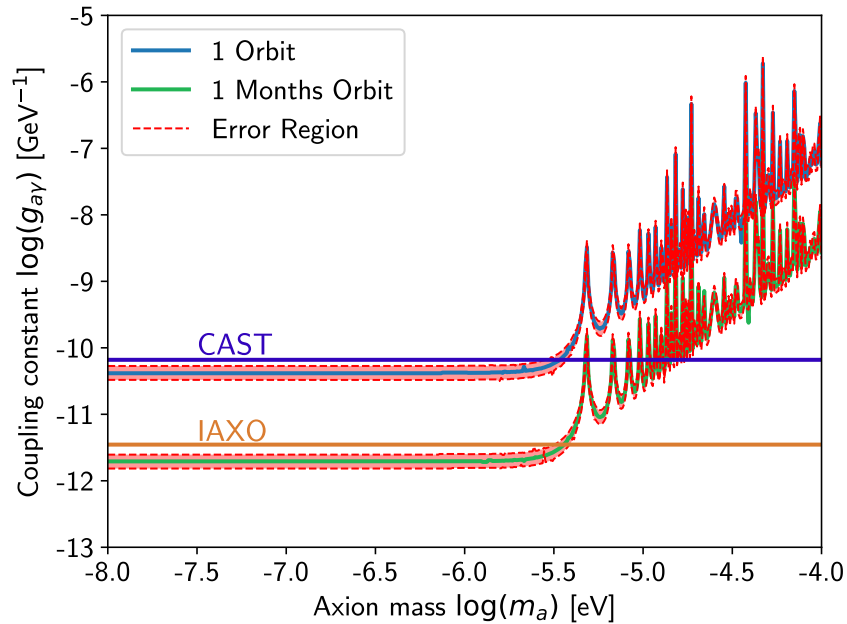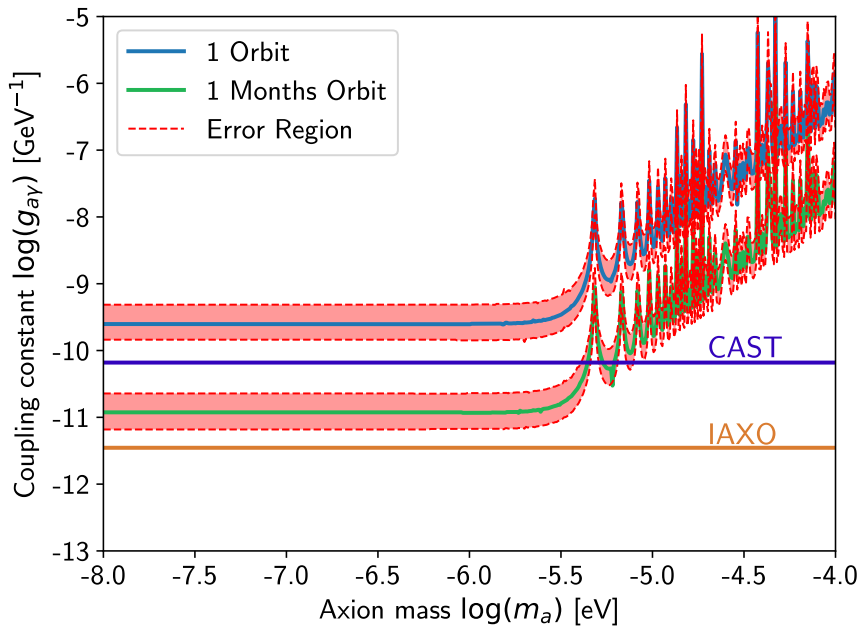
Figure 14: Minimum coupling strength $g_{a\gamma}$ able to produce a single photon difference in photon detection for pseudoscalar ALPs after a single orbit and a month of equatorial orbit as a function of axion mass $m_a$.

For the equatorial orbit, figure 14 shows that for pseudoscalar ALPs, the maximum constraint on the coupling constant possible after a month of orbit is $g_{a\gamma} < (1.3 \pm 1.0) \times 10^{-11}$ GeV$^{-1}$.

# 9    Discussion

In this investigation we have demonstrates that through the exchange of photons between a pair of satellites in orbit of the Earth, it should be possible to generate better constraints on the coupling between photons and ALPs than the current best experiments for masses $m_a \approx 3 \times 10^{-6}$eV. Figure 13 demonstrates an ability to outperform both CAST and it's upcoming successor IAXO it's ability to constrain the photons coupling to pseudoscalar ALPs. Additionally, from figure 12 we see that this method could also outperform both ALPS-I and the upcoming ALPS-II in its ability to constrain the coupling to scalar axion-like particles. The lunar laser experiment, however, is less successful and falls short of the limits achieved by CAST by several orders of magnitude.

There are clear advantages to using the satellite experiments when compared to many of the current axion searching methods. Unlike CAST and IAXO the polar orbit can also search for scalar ALPs. Additionally, while ADMX requires that ALPs not only exist but form a significant contribution of dark matter, a requirement that neither of our methods shares. Both of our methods have more in common with the 'light shining through walls' experiments, which can detect both scalar and pseudoscalar ALPs. However, we require only a single axion-photon conversion rather than two, increasing the effectiveness of the experiment.

The limits calculated for both the Lunar laser and satellite experiments are likely to be overestimates for the capability of this type of system due to simplifications and assumptions

we have used. For further study into the viability of these axion detection experiments, there are many factors that would need to be expanded upon and considered to make the modelling more accurate. These can be separated in two parts, one for improving the magnetic field modelling and the other for improving the realism of the lunar laser and satellite experiments.

The dipole approximation of the Earth's field has been shown to closely resemble experimental measurements. However, since a single value for the magnetic field at the equator $B_0$ is used, the model neglects changes in the field due to variations in the field strength at the surface arising from the specific composition of the geodynamo [29] and local palaeomagnetism [34]. This variation would have an important impact on the probability of axion production in long distance photon beams and therefore should be considered in future investigations.

The precision of our toy model for the magnetic field contributions of the solar wind could be improved by considering a greater area of space with a larger density of segments. This however greatly increases the time required to compute the field. The process could be made more efficient by making use of the systems rotational symmetry about the z-axis. Additionally, the density of segments could be dynamically chosen such that the density is higher nearer to the Earth.

The solar wind model used assumes that the solar wind acts as an incompressible fluid. This requires that the material density is constant which is known not to be true [33]. It also neglects key magnetospheric features such as the current ring, equatorial current sheet and field-aligned currents, as well as the tilt of the Earth's axis relative to the heliocentric radius. However, the model used should be sufficient to predict the gross contribution of the solar wind, particularly at the low altitudes considered in this investigation. The additional contributions mentioned above would only have a notable impact on the direction of the magnetic field in the area local to the satellites. A better model could be built by solving the three-dimensional magnetohydrodynamics (MHD) equations [35]. The most convenient and physically accurate solution would, however, be to use an existing semi-empirical model such as that developed by Tsyganenko since these models much more accurately portray the magnetic field strength and direction due to all sources [36].

Efforts were made to ensure both the lunar laser and satellite models were as accurate as possible, however, there were some simplifications made that would need to be addressed in future studies on this topic. For the lunar laser experiment we realise that in order to take model the photon detection over the course of a full night of five hours, we have to consider the changes to beam divergence caused by the angular component of the beam as it tracks the moon across the night sky. If we wished to still neglect the complications caused by a changing angle then we would have to reduce the measurement time and therefore the number of photons we can detect each night. We also idealised the location of our telescope and reflector to simplify the calculations. If further studies were to select an existing location then an angular component would also be included. However, the selection of an existing location at altitude would bring a positive effect to the results as the atmospheric turbulence has a greater effect on the beam divergence at lower altitudes, where the atmosphere has a greater density. We could improve upon the transmission of the laser through the atmosphere further by using light of a larger wavelength such as infra-red. There would need to be a compromise on this, however, as larger wavelengths have smaller beam divergences as they propagate through the atmosphere but have a greater divergence when propagating through a vacuum. We are also limited as to which wavelengths we may use, however, as the reflectors must be capable of returning the signal to earth with as little divergence as possible.

An important issue to be addressed is that we have ignored any other sources of photons

that will add a significant error to both experiments such as solar photons. In the lunar laser ranging experiments, there is a large amount of background noise caused by photons being is detected due to external photon sources. This makes it difficult to identify which photons were echoes of the source laser. For example, during periods of a full moon, this background noise is large enough to reduce the signal to noise ratio so much that the experiment is rendered invalid for most telescopes. APOLLO is one of the few that can still operate. Additionally, the signal strength is reduced by a factor of ten during this time [37]. A further challenge experienced during the full moon is that many reflectors become distorted by solar heating which increases the divergence of the returning laser [38]. During the new moon periods, the lunar laser telescopes face the challenge of the lunar surface not being sufficiently visible to allow for accurate location of the reflectors. To cope with this, the measurements must be taken near the moon is illuminated, increasing the signal to noise ratio. The sum of these issues is that for our lunar laser experiment we would have to reduce the time available to collect data or expand significantly upon our model. We also made the assumption that a single difference in the number of photons would be measurable. The high levels of background noise show that this is unrealistic even if the technology were available. There are ways to reduce the signal to noise ratio, however, such as using a polarised laser and adding filters to the telescopes that are tuned to the specific wavelength and polarisation of the laser in use.

For the satellite experiment, greater axion production probabilities could be achieved by orbiting satellites around a stronger magnetic field source. Jupiter, for example, has a dipole moment 20,000 times larger than that of Earth with a dipole equatorial field of 0.428mT [39]. Since the magnetic field at the equator is around 14 times greater than that of Earth and the probability of axion production scales as the square of the magnetic field (equation (5)), satellites orbiting Jupiter would be around 144 times more effective at constraining the axion-photon coupling constant than satellites orbiting Earth. The magnetic field strength incident on the beams could also be improved by reducing the orbital altitude. Additionally, the production probabilities could be increased by extending the length of the photon beam. This would mean either discarding our assumption that every photon emitted will reach the detector or increasing the detector size. The former option would force us to calculate the beam divergence and the ratio of emitted to received photons whereas for the latter option we are only bound by the technology available. Unlike the lunar laser experiment, when selecting an appropriate wavelength there is no trade-off between one that propagates through a vacuum more easily and one that is less affected by atmospheric turbulence. Neither are we limited to wavelengths of light capable of being reflected by the reflectors on the lunar surface. This grants us more freedom in experimenting with different wavelengths of light to find the most ideal for axion detection. In order to increase the length of the system, it would be advantageous to use light of a smaller wavelength to reduce beam divergence and thus increase the number of detected photons.

Background noise due to solar photons must also be considered for the satellite experiment. Again this background noise could be greatly restricted through the implementation of filters and the polarisation of the laser in use. Both experiments would benefit from the additions of a more powerful laser and a larger photon collection area to increase the number of photons detected. By using the same method as for the rest of the investigation but implementing a 4m diameter photon collecting area and a 2W laser. We calculate that for the polar orbit case, after one month of a constraint of $g_{a\gamma} < 2 \times 10^{-13}$GeV$^{-1}$ could be achieved.

## 10    Conclusion

We have investigated two new methods for improving the constraints on the axion-photon coupling constant by using the geomagnetic field. This field was modelled as a superposition of the Earth's dipole field and the field due to the solar wind interacting with the magnetosphere. The field due to the solar wind was calculated by modelling the solar wind as an incomprehensible, charged fluid flowing over a Rankine halfbody. Using a computer simulation that separates the field into discrete sections of constant field, the probability of photons being converted into axions could then be calculated.

We considered the possibility of utilising the reflectors on the lunar surface to return an emitted photon beam back to the source on Earth and measure the number of returning photons. The eccentricity in the lunar orbital radius changes the probability of a conversion taking place before the photon returns to Earth. This change in probability allows us to constrain the coupling constant. Using the experimental parameters of the APOLLO lunar ranging experiment we were able to estimate the theoretical best limit of $g_{a\gamma} < (7.2 \pm 1.9) \times 10^{-5} \text{GeV}^{-1}$ for pseudoscalar ALPs with masses in the range $m_a < 10^{-7} \text{eV}$.

The second method considered sending a photon beam between a pair of satellites 125km apart, orbiting the Earth in either a polar or equatorial orbit. The change in the magnitude of the relevant component of the magnetic field results in a periodic change in the probability of photons converting to ALPs as they travel between the satellites. Using the experimental parameters of the LISA Pathfinder experiment, for the polar orbit we were able to estimate a best limit constraint of $g_{a\gamma} < (2.0 \pm 0.5) \times 10^{-12} \text{ GeV}^{-1}$ for pseudoscalar ALPs and $g'_{a\gamma} < (4.0 \pm 1.0) \times 10^{-12} \text{ GeV}^{-1}$ for scalar ALPs. Both with masses in the range $m_a < 2 \times 10^{-6} \text{ eV}$ and both results produced after one month of orbit. We also estimate that such a satellite pair in an equatorial orbit would be able to produce constraints of $g_{a\gamma} < (1.3 \pm 1.0) \times 10^{-11} \text{GeV}^{-1}$ for pseudoscalar ALPs for the same mass range.

The constraints for the lunar laser case are orders of magnitude worse than those produced by CAST or those expected be produced by IAXO. Considering the simplifications we made to this model it is unlikely that this method will be improved in a significant enough manner to produce competitive constraints in the future. The constraints on pseudoscalar ALPs produced by the satellite cases outperform CAST and IAXO. The constraints on scalar ALPs produced by the polar orbit also outperform those of the current best experiment, ALPS. For both scalar and pseudoscalar ALPs, there is a lot of potential for the development of this experiment to search for axions and ALPs.

## References

[1]  R.D. Peccei and H.R. Quinn. "CP conservation in the presence of pseudoparticles". In: *Physical Review Letters* 38.25 (1977), pp. 1440–1443. ISSN: 00319007.

[2]  Georg Raffelt. "Axions". eng. In: *Space Science Reviews* 100.1 (Jan. 2002), pp. 153–158. ISSN: 0038-6308.

[3]  Jm Pendlebury et al. "Revised experimental upper limit on the electric dipole moment of the neutron". English. In: *Physical Review D* 92.9 (Nov. 2015). ISSN: 2470-0010.

[4]  C. Abel et al. "Search for axionlike dark matter through nuclear spin precession in electric and magnetic fields". In: *Physical Review X* 7.4 (Nov. 2017). ISSN: 21603308.

[5]  Andreas Ringwald. "Exploring the role of axions and other WISPs in the dark universe". eng. In: *Physics of the Dark Universe* 1.1-2 (2012), pp. 116–135. ISSN: 2212-6864.

[6]  Leszek Roszkowski, Enrico Sessolo, and Sebastian Trojanowski. "WIMP dark matter candidates and searches – current status and future prospects". eng. In: *Reports on progress in physics. Physical Society (Great Britain)* (2018). ISSN: 1361-6633.

[7]  Laura Baudis. "WIMP dark matter direct-detection searches in noble gases". eng. In: *Physics of the Dark Universe* 4 (2014), pp. 50–59. ISSN: 2212-6864.

[8]  Georg Raffelt and Leo Stodolsky. "Mixing of the photon with low-mass particles". In: *Phys. Rev. D* 37 (5 Mar. 1988), pp. 1237–1249. DOI: 10.1103/PhysRevD.37.1237. URL: https://link.aps.org/doi/10.1103/PhysRevD.37.1237.

[9]  P Svrcek and E Witten. "Axions in string theory". English. In: *Journal Of High Energy Physics* 6 (June 2006). ISSN: 1029-8479.

[10]  MI Cherry. "Stars as laboratories for fundamental physics - Raffelt,GG". English. In: *Nature* 384.6605 (1996), pp. 128–128. ISSN: 0028-0836.

[11]  P. Sikivie. "Experimental Tests of the "Invisible" Axion". In: *Phys. Rev. Lett.* 51 (16 Oct. 1983), pp. 1415–1417. DOI: 10.1103/PhysRevLett.51.1415. URL: https://link.aps.org/doi/10.1103/PhysRevLett.51.141.

[12]  Klaus Ehret et al. "New ALPS results on hidden-sector lightweights". eng. In: *Physics Letters B* 689.4-5 (May 2010), pp. 149–155. ISSN: 0370-2693.

[13]  V. Anastassopoulos et al. "New CAST limit on the axionphoton interaction". In: *Nature Physics* 13.6 (May 2017). ISSN: 1745-2473.

[14]  K. Freese, M. Lisanti, and C. Savage. "Colloquium: Annual modulation of dark matter". In: *Reviews of Modern Physics* 85.4 (Nov. 2013), pp. 1561–1581. ISSN: 00346861.

[15]  S. J. Asztalos et al. "SQUID-Based Microwave Cavity Search for Dark-Matter Axions". In: *Phys. Rev. Lett.* 104 (4 Jan. 2010), p. 041301. DOI: 10.1103/PhysRevLett.104.041301. URL: https://link.aps.org/doi/10.1103/PhysRevLett.104.041301.

[16]  T. Dafni et al. "An update on the Axion Helioscopes front: current activities at CAST and the IAXO project". eng. In: *Nuclear and Particle Physics Proceedings* 273-275 (2016), pp. 244–249. ISSN: 2405-6014.

[17]  E Armengaud et al. "Conceptual design of the International Axion Observatory (IAXO)". In: *Journal of Instrumentation* 9.05 (2014), T05002. URL: http://stacks.iop.org/1748-0221/9/i=05/a=T05002.

[18]  R Bähre. "any light particle search ii technical design report". eng. In: *Journal of Instrumentation* 8.09 (Sept. 2013), T09001–T09001. ISSN: 1748-0221.

[19]  G.G. Raffelt. *Stars as Laboratories for Fundamental Physics: The Astrophysics of Neutrinos, Axions, and Other Weakly Interacting Particles*. Theoretical Astrophysics. University of Chicago Press, 1996. ISBN: 9780226702728. URL: `https://books.google.co.uk/books?id=6esnbt7BfIwC`.

[20]  Raffelt and Stodolsky. "Mixing of the photon with low-mass particles". eng. In: *Physical review. D, Particles and fields* 37.5 (1988). ISSN: 0556-2821.

[21]  T W Murphy. "Lunar laser ranging: the millimeter challenge". eng. In: *Reports on Progress in Physics* 76.7 (2013). ISSN: 0034-4885.

[22]  C Courde et al. "Lunar laser ranging in infrared at the Grasse laser station". English. In: *Astronomy  Astrophysics* 602 (2017). ISSN: 1432-0746.

[23]  Infrared Information Environmental Research Institute of Michigan and Analysis (Iria) Center. *The infrared handbook*. The Office, 1978. ISBN: 096035901X. URL: `http://hdl.handle.net/2027/mdp.39015002093360`.

[24]  George C. Valley. "Isoplanatic degradation of tilt correction and short-term imaging systems". In: *Appl. Opt.* 19.4 (1980), pp. 574–577. DOI: `10.1364/AO.19.000574`. URL: `http://ao.osa.org/abstract.cfm?URI=ao-19-4-574`.

[25]  I. de Pater and J.J. Lissauer. *Planetary Sciences*. Cambridge University Press, 2001. ISBN: 9780521482196. URL: `https://books.google.co.uk/books?id=RaJdy3\_VINQC`.

[26]  T.W. Murphy Jr. et al. "The apache point observatory lunar laser-ranging operation: Instrument description and first detections". In: *Publications of the Astronomical Society of the Pacific* 120.863 (2008), pp. 20–37. ISSN: 00046280.

[27]  P. W. McNamara and LISA Pathfinder Team. "LISA Pathfinder". In: *AIP Conference Proceedings* 873.1 (2006), pp. 49–58. DOI: `10.1063/1.2405021`. eprint: `https://aip.scitation.org/doi/pdf/10.1063/1.2405021`. URL: `https://aip.scitation.org/doi/abs/10.1063/1.2405021`.

[28]  D. A Shaddock. "An Overview of the Laser Interferometer Space Antenna". eng. In: *Publications of the Astronomical Society of Australia* 26.2 (2009), pp. 128–132. ISSN: 1323-3580.

[29]  Nigel Weiss. "Dynamos in planets, stars and galaxies". In: *Astronomy and Geophysics* 43.3 (2002). ISSN: 1366-8781.

[30]  Imke de Pater and Jack J. Lissauer. *Planetary Sciences*. 2nd ed. Cambridge University Press, 2010. DOI: `10.1017/CBO9780511780561`.

[31]  A. Chulliat et al. "The US/UK World Magnetic Model for 2015-2020". NOAA National Geophysical Data Center. 2018.

[32]  Wolfgang Baumjohann et al. "Current Systems in Planetary Magnetospheres and Ionospheres". In: *Space Science Reviews* 152.1 (2010), pp. 99–134. ISSN: 1572-9672. DOI: `10.1007/s11214-010-9629-z`. URL: `https://doi.org/10.1007/s11214-010-9629-z`.

[33]   Carolus J. Schrijver et al. *Heliophysics: Plasma Physics of the Local Cosmos*. Ed. by Carolus J. Schrijver and George L. Siscoe. Cambridge, UK: Cambridge University Press, Aug. 2011. Chap. 3, pp. 43–44. URL: `http://www.cambridge.org/us/academic/subjects/earth-and-environmental-science/atmospheric-science-and-meteorology/heliophysics-plasma-physics-local-cosmos`.

[34]   W. Lowrie. *Fundamentals of Geophysics*. Cambridge University Press, 2007. ISBN: 9781139465953. URL: `https://books.google.co.uk/books?id=h2-NjUg4RtEC`.

[35]   C. Wu, R. Walker, and J Dawson. "A three dimensional MHD model of the Earths magnetosphere". In: *Geophysical Research Letters* 8.5 (1981), pp. 523–526. ISSN: 0094-8276.

[36]   N. A. Tsyganenko. "Databased modeling of the geomagnetosphere with an IMFdependent magnetopause". In: *Journal of Geophysical Research: Space Physics* 119.1 (2014), pp. 335–354. ISSN: 2169-9380.

[37]   T.W. Murphy et al. "Lunar eclipse observations reveal anomalous thermal performance of Apollo reflectors". eng. In: *Icarus* 231 (2014), pp. 183–192. ISSN: 0019-1035.

[38]   T.W. Murphy et al. "Long-term degradation of optical devices on the Moon". eng. In: *Icarus* 208.1 (2010), pp. 31–35. ISSN: 0019-1035.

[39]   Norman Ness. "Space Exploration of Planetary Magnetism". eng. In: *Space Science Reviews* 152.1 (2010), pp. 5–22. ISSN: 0038-6308.